JOURNAL OF MATERIALS SCIENCE 27 (1992) 616–624

Microstructure of zirconia–yttria plasma-sprayed thermal barrier coatings

P. D. HARMSWORTH*, R. STEVENS
School of Materials, University of Leeds, Leeds LS2, 9JT, UK

The objective of this paper is to report on the characterization of the highly complex microstructure of zirconia coatings, which arise as a result of the plasma-spraying process. The fine structure has been observed to change through the thickness of the coating, behaviour which has been related to the cooling rate and crystallization of the deposited material. Microstructural features such as an amorphous bond coat/ceramic interfacial film and a grain-boundary glassy phase, which are believed to have a significant effect upon coating properties such as adhesion and compliance, have been shown to be present.

1. Introduction

Early work on thermal barriers demonstrated the advantages of plasma-sprayed zirconia coatings [1] as a short-term solution to increasing gas turbine operating temperatures. The viability of such coatings has already been proven, as evidenced by their introduction into the after-burner sections of many high-performance engines. Recently, research has concentrated on the durability and thermal cycle life of the coatings, mainly through the development of the plasma-spraying process, to introduce coated components into more critical, highly stressed regions of the gas turbine engine. Improved performance and durability can be achieved by optimizing the zirconia stabilizer content within the range 6–10 wt % yttria. These studies [2, 3] have been of an empirical nature, based upon thermal cycle rig tests, an accepted test method in thermal barrier development. The use of such tests does not, however, provide any explanation of the mechanisms by which such coating compositions improve performance.

Analysis of the optimum coating compositions has shown them to correspond to a peak in the metastable t′ tetragonal phase content. The improved performance has consequently been linked to the properties of this t′ phase [4]. Thermal cycling and static ageing experiments have shown that a high-temperature destabilization of the t′ phase can occur, resulting in equilibrium t and c phases, with the t phase transforming to m symmetry after long periods. The 3%–5% volume expansion and ~ 10% shear strains associated with this transformation were believed to have a life-limiting effect on coating performance, eventually leading to spallation. Coating durability was therefore believed to be determined by the residual content of t′ phase.

Few detailed studies have been made into the microstructure of plasma-sprayed zirconia coatings and into possible microstructure–property relationships. Furthermore, investigations of how the microstructure is related to and changed with service exposure, particularly the high-temperature destabilization of the t′ phase, are not extensive. The absence of such investigations is surprising, because such information would be helpful in explaining the mechanisms of adhesion and why particular coating compositions exhibit improved durability.

The present paper reports on a systematic microstructural and phase analysis of as-received coatings, within the optimum stabilizer range. We demonstrate the build-up of the plasma-sprayed coating structure and have investigated the changes in coating microstructure through the thickness of the coating.

2. Experimental methods and materials

2.1. Plasma-sprayed coating conditions

All the coatings were plasma sprayed at Rolls Royce, Derby, using standardized spray conditions.

In order to obtain a constant flow rate during spraying, the nozzle needed to be in good condition and in the case of zirconia, the powder to be dry. The substrate was a 5 cm square, 3 mm thick, nimonic alloy, which was initially grit blasted to increase surface roughness and to remove surface oxides or other impurities.

A metallic bond layer of the MCrAlY composition, where M = Ni or Co, was initially deposited by plasma. The zirconia coating was then sprayed over this layer shortly afterwards, forming the standard duplex structure.

2.2. Cross-sectional foil preparation

Preparation of cross-sectional TEM foils was developed from published techniques for the examination of coatings [5, 6]. Such techniques had

*Present address: Tioxide Group plc, Central Laboratories, Portrack Lane, Stockton-on-Tees, UK.

0022–2461/92 $03.00 + .12

TABLE I Analysis of MEL SCY8 powder as a percentage

Y_2O_3	SiO_2	TiO_2	Fe_2O_3	SO_3	ZrO_2
8.2	0.08	0.1	0.08	0.005	Balance

themselves been adapted from methods for examining oxide films [7, 8].

The initial microstructural characterization was based on four coating compositions which had been found to be in the range for optimum performance in thermal cycle rigs. The coating compositions investigated comprised ZrO_2 with 6, 8, 10 and 12 wt % Y_2O_3 and were plasma sprayed from commercially available MEL SC or high-purity grade powders (see Table I).

2.3. SEM characterization

Characterization of polished coating cross-sections was found useful in providing the following information:

1. the degree of particle melting and an approximation of the porosity in the coating;
2. the level of segmentation cracking, which gives a measure of the coating integrity;
3. the morphology of the bond coat/ceramic interface.

An examination such as described can therefore be used as a quick method to help develop the plasma-spraying process, to increase the degree of particle melting and thus improve coating morphology.

Analysis of polished cross-sections has limitations, in that the nature of the coating structure can easily be damaged during sectioning, mounting, and in the polishing procedures [9]. Even after careful preparation much of the information regarding the fine microstructure becomes lost during polishing. Furthermore all coatings, regardless of composition, appeared similar when examined in this manner, revealing little distinction between different compositions and processing conditions.

2.4. Fractography

Detailed information about the structure could only be gained by examination of the surface after controlled fracture of a coating which had been removed from the substrate [10]. A typical fracture surface is illustrated in Fig. 1, which shows the coatings to be built up from layers of material in the form of lamellae. The lamellae are invariably aligned parallel to the substrate, and assume the irregular surface characteristics of previously deposited material. Lamellar dimensions vary, ranging from $\sim 6\,\mu m$ thick towards the centre, to less than 1 μm at the periphery. The length of the lamellae can extend up to $\sim 100\,\mu m$, although for individual lamellae the length is often restricted by the topography of previously deposited material.

The fracture path of the coating follows preferentially the line of the interface between the lamellae, Fig. 2, suggesting weak interlamellar adhesion. This is

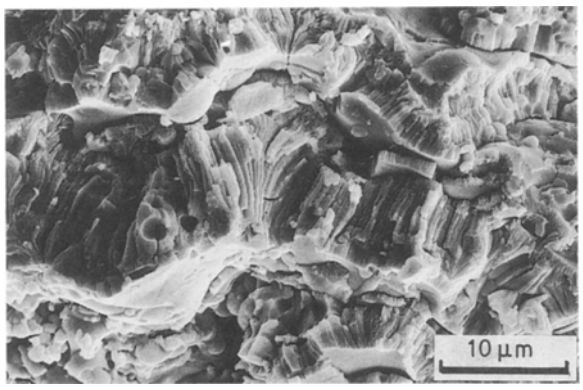

Figure 1 Scanning electron micrograph of coating fracture surface, showing lamellar nature of the coating and fine columnar grain structure. Also shown is evidence of porosity, enclosed within individual lamellae.

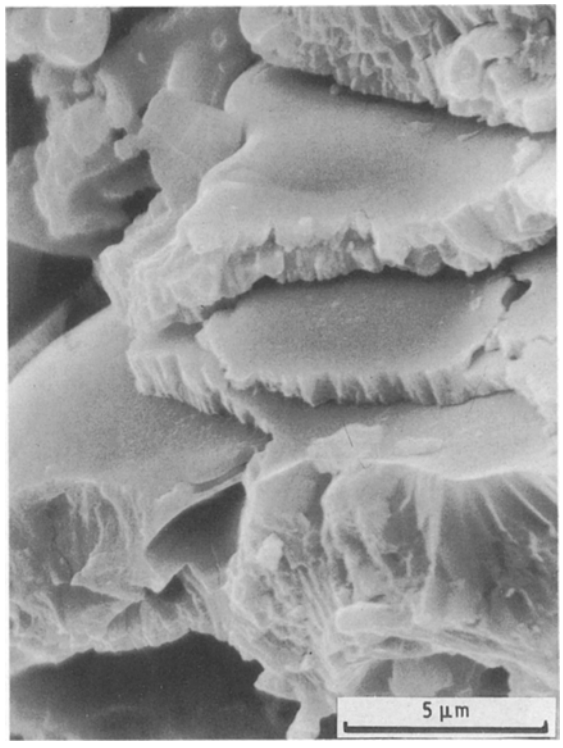

Figure 2 SEM fracture surface showing the preferential interlamellar fracture.

believed to arise from an intermittent contact area between the lamellae, due to a thin layer of interlamellar porosity. This fracture mode also indicates that solidification occurs in a discontinuous manner, deposited material completely solidifying to form the lamellae prior to the impact of subsequent material, as interdiffusion has not been observed between lamellae. Porosity of this type is often observed in materials plasma sprayed in air and is believed to arise from the entrapment of the air during the plasma deposition. Fabrication at low pressures or in a vacuum, for example, has been shown [11] to reduce such porosity significantly.

Fracture of the lamellae normally occurs intergranularly. Such a failure mode indicates weak intergranular bonding exists between the grains, suggesting

the presence of a thin intergranular glassy phase. The microstructures of fractured lamellae are shown in Figs 1 and 3 and comprise a mixture of: (1) fine columnar grains, 0.1–1 μm diameter and up to 4 μm long, nucleating at lamellae interfaces which grow in a direction perpendicular to the lamellae boundary, that is, in the direction of greatest heat flow, and can often completely traverse the lamellae; (2) equiaxed grains of up to 1 μm diameter, occurring only in lamellae situated between the centre and the outer surface of the coating.

Also observed within the fractured lamellar surface were totally enclosed spherical pores ~ 1 μm diameter. This form of porosity is believed to arise from the evolution of absorbed gases during plasma spraying [11]. Variations of the lamellar microstructure through the thickness of the coating are difficult to quantify from examination of the fracture surface due to its irregular nature. Much finer and shorter columnar grains, 0.1 μm × 1 μm, can however be identified in the coating at the interface with the bond coat, Fig. 4.

2.5. TEM characterization

The most straightforward TEM analysis is that of planar sections taken from coatings removed from the substrate by chemical methods. This form of two-dimensional analysis has a number of limitations, principally that it cannot account for grain orientations perpendicular to the substrate surface, and secondly, changes in coating structure through the coating thickness cannot be assessed. Fig. 5 shows how the microstructure of the foils tends to be of fine equiaxed grains ranging in size from 0.1–1 μm, slightly elongated in some instances. These structures do not easily relate to the fracture surface analysis presented previously. The microstructure represents a cross-section through a number of columnar grains in a single lamella.

The correlation between the TEM microstructural observations and those of the fracture surfaces was improved by devising a foil preparation technique which allowed investigation of coating cross-sections. This form of analysis proved highly successful for examination of the highly orientated lamellar microstructure and also the changes in microstructure through the coating thickness.

A typical TEM section through a series of lamellae is shown in Fig. 6. The lamellae are ~ 0.5 μm thick, and orientated approximately parallel to the substrate surface, although of necessity they follow the exact

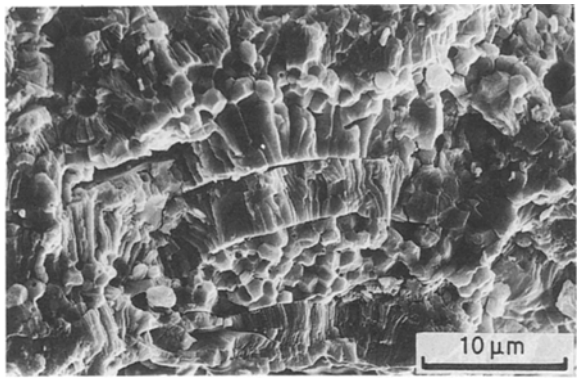

Figure 3 SEM fracture surface showing variety of lamellar microstructures composed of fine and coarse columnar grains and equiaxed grains of ~ 1 μm.

Figure 4 SEM fracture surface of interface with bond layer showing a very fine columnar grain structure for lamellae at the interface.

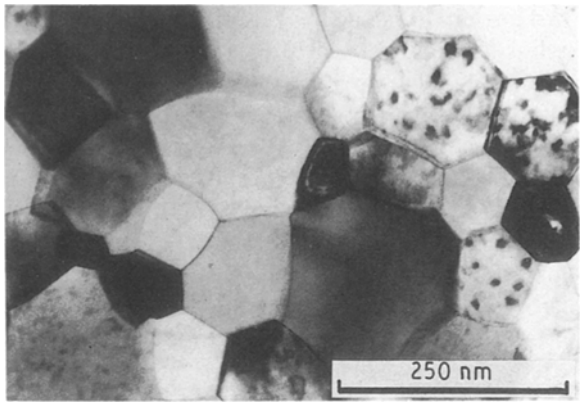

Figure 5 TEM planar section through the coating, showing a section through the columnar grains in a lamella.

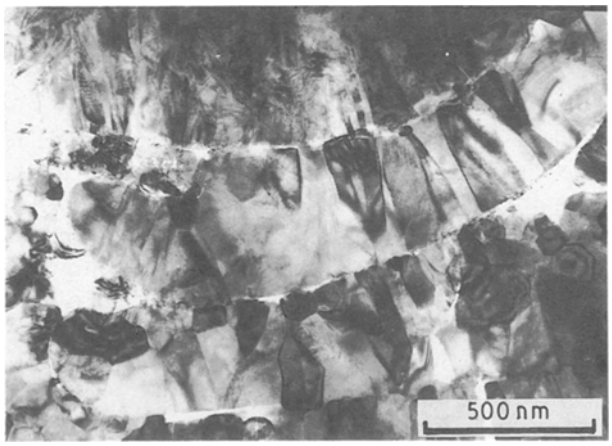

Figure 6 TEM cross-section through a series of lamellae showing the fine columnar grain structure orientated perpendicular to the lamellar interface.

contours of previously deposited material. The microstructure of the lamellae is composed of fine columnar grains of 0.1 μm × 0.5 μm cross-section, orientated perpendicular to the substrate interface. Fig. 7 shows another lamellar region where the individual deposits are over 1 μm thick. These thicker lamellae arise where there was reduced spread of molten ceramic material on impact. The lamellae in Fig. 7 are also composed of fine columnar grains 0.2 μm thick, by up to 1 μm in length. The lamellae microstructure was not composed entirely of parallel columnar grains which had nucleated on the impact interface and grown through the molten splat to the opposite interface. Often evidence for nucleation on both sides of the splat could be identified, the resultant grains intersecting at a point within the lamellae.

Grain growth across the lamellar interfaces was not observed in these sections, suggesting solidification of deposited material is complete prior to the impact of a subsequent molten droplet. The lamellar interface was often found to be discontinuous, giving rise to a thin film of interlamellar porosity, 0.1–0.2 μm thick, along which preferential fracture of the coatings was observed to take place.

2.6. Formation of coating microstructure

SEM and TEM analysis has shown the coatings to have a lamellar structure, which has been found to be a characteristic feature of the plasma-sprayed materials [12]. Powder injected into the plasma is melted and accelerated, forming a molten globule [13]. On impacting the substrate, a molten splat forms and spreads out across the surface, cooling rapidly, and solidifies to form the lamellae. The outer surface of the coating, Fig. 8, shows the outline of a solidified splat, which has spread out, fragmenting at its periphery [14].

The degree of splat spreading and variation in lamellar thickness is controlled by a number of factors [15, 16], such as droplet temperature, viscosity, velocity of impact, and wetting behaviour between the splat and the previously deposited material. The molten splat then cools rapidly by heat conduction into the heat sink of the substrate or into the surrounding air [17]. On cooling below T_m, solidification commences, preventing further spread of material. The thickness of each of the lamellae is therefore dependent upon the amount of molten splat spread across the uneven surface prior to solidification. Consequently, lamellae are generally thicker at their centre and thinner at their periphery with the shape dependent on the flow pattern of the molten material on impact.

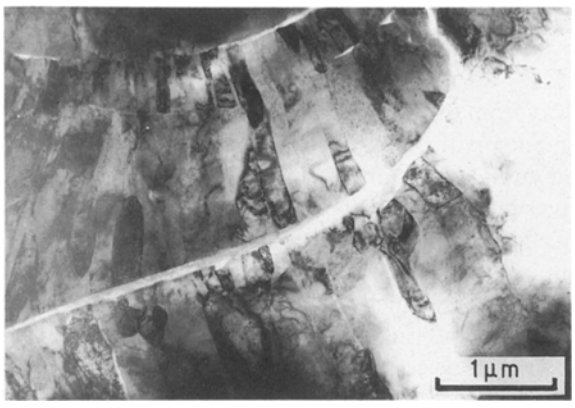

Figure 7 TEM cross-section showing the variation in the lamellar thickness and grain size. Note the presence of much larger columnar grain than Fig. 8 and a thin layer of interlamellar porosity.

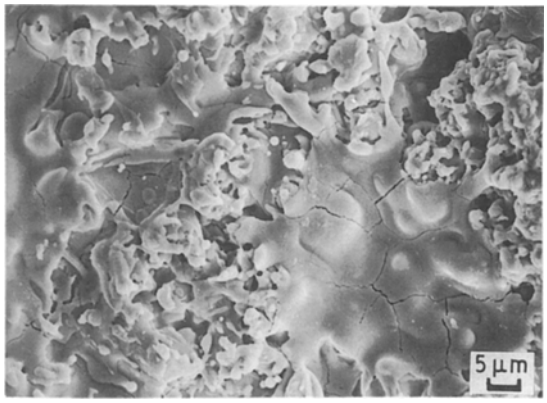

Figure 8 Scanning electron micrograph of a solidified splat on the surface of the coating which gives rise to the lamellar structure.

The microstructure of the lamellae is believed to be determined by the rate and direction of greatest heat removal from the deposited material and its mode of crystallization [16]. Columnar grain growth arises from heterogeneous nucleation at splat boundaries [18], and rapid growth into the molten splat. Alternatively fine equiaxed grains can form as a result of homogeneous nucleation and precipitation from a highly undercooled melt. The undercooling necessary for homogeneous nucleation is taken to be $\sim 0.2\,T_m$ [19]. This is within the estimated cooling rates for plasma-sprayed material of up to $10^6\,K\,s^{-1}$ [20]. Homogeneous nucleation would, however, result in very fine (< 0.1 μm diameter) grains, due to the high nucleation and low growth rates. Such structures have been observed in isolated instances in the present coatings using TEM, Fig. 9.

2.7. Variation in structure through coating thickness

The method used to produce cross-sectional TEM foils allowed investigation of the coating structure from the bond coat interface through to the outer surface of the coating.

2.7.1. Bond coat–ceramic interface

The foil preparation technique allowed thinning of the interfacial region between the bond coat and the

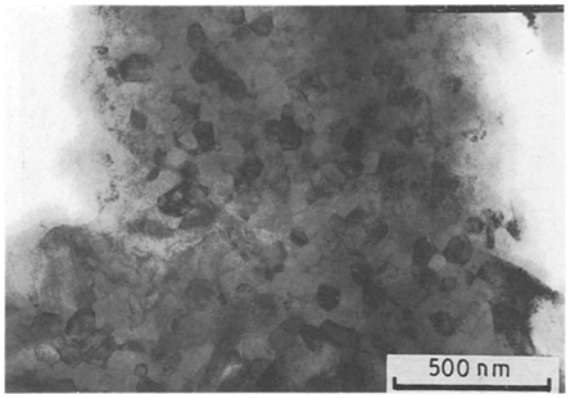

Figure 9 Transmission electron micrograph of isolated area composed of ultra-fine < 0.1 μm equiaxed grains, possibly the result of homogeneous nucleation.

ceramic. Examination in TEM of such foils has shown that a thin interfacial amorphous film ranging in thickness from 50–200 nm exists between these two layers, shown in Fig. 10. This thin layer could not always be imaged, as often it was preferentially etched away during ion-beam thinning, leaving a gap between the bond coat and the ceramic. The amorphous nature of this interfacial layer was demonstrated by selected-area diffraction, shown in Fig. 11a, which shows a pattern with a series of faint diffuse rings [21]. The intensity of the rings is low due to the small volume of material typically < 50 nm across, which gives rise to electron diffraction. By imaging part of a ring in dark field, Fig. 11b, the interfacial region can be illuminated, revealing the continuous nature of this thin layer.

Qualitative microanalysis using STEM revealed the change in chemical composition across the interfacial region between ceramic and bond coat, Fig. 12. The micrographs in Fig. 12 show a thicker interfacial amorphous layer due to a reduced angle of cross-section. The elemental compositions of each layer across the interface are shown in the EDX micro-

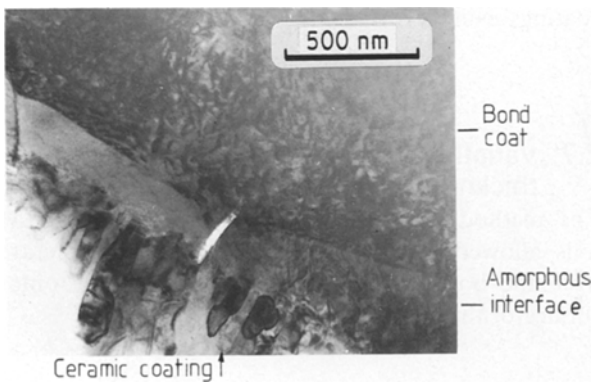

Figure 10 TEM cross-section of the ceramic/bond coat interface, showing the amorphous bond coat/ceramic interfacial region. Also shown are fine columnar grains emanating from this region into the ceramic.

analysis traces of Fig. 12b–d. Trace 1 is from the fine-grained ceramic region adjacent to the interface, and indicates that small amounts of Ni and Cr diffusion have occurred, from the bond coat into the ceramic. Trace 2 is representative of the amorphous interfacial layer adjacent to the ceramic; it is found to be rich in Ni with remnant amounts of Zr and Y, and possibly some Si, although this is partially obscured by the Zr and Y peaks. Trace 3 is from the bond coat adjacent to the amorphous layer, where there is an increased presence of Cr and also some Al, related to the NiCrAl composition of the bond layer.

The formation of this amorphous phase is believed to be a consequence of the plasma-spraying process. The first molten splats to impact the substrate need to have been heated to temperatures in excess of 3000 °C [22]. These splats are instantly solidified on impact with the substrate and so will undergo the most severe cooling regime. The impact of this "superheated" molten ceramic with the relatively low melting point bond layer is believed to result in a fusion between the two, caused by the partial melting and rapid quenching of the outer surface of the bond coat. This forms the thin amorphous boundary film, composed largely of bond coat together with some ceramic material. The presence of impurities such as SiO_2 in the starting powder, together with oxidation products of the bond layer, are also believed to have a significant effect in aiding the formation of the amorphous phase, although this was difficult to detect using EDX.

Growing out of this amorphous film into the ceramic layer are fine columnar grains, approximately 50 nm diameter, by up to 200 nm long. The structure beyond these columnar grains continues to develop by means of a series of nucleation and growth stages. This indicates a reduced rate of cooling, resulting in slower nucleation and growth rates in the rest of the splat due to the insulation provided by the layer in contact with the bond coat. Cracking can often be observed between the fine columnar grains and the rest of the lamellae, see Fig. 11. It is likely to arise due to differential thermal contraction rates between the initially deposited and rapidly cooled fine-grain material, and the rest of the splat which is cooled more slowly. If the stresses arising from the differential rates of contraction are sufficient, then cracking can result.

2.7.2. Variation in grain size

Away from the bond coat interface, the microstructure is made up of a combination of much larger columnar and equiaxed grains having diameters > 1 μm. This larger grain size is believed to result from the insulating effect of previously deposited material, i.e. a reduction in the cooling rate results in a lower driving force for nucleation which promotes grain growth. Towards the centre and outer surface of the coating, deposited material may not have completely solidified prior to the impact of the subsequent splat. This possibility arises due to: (1) the good thermal insulation of previously deposited material with a thickness of 200 μm; (2) up to 50 μm may be deposited in one pass of the

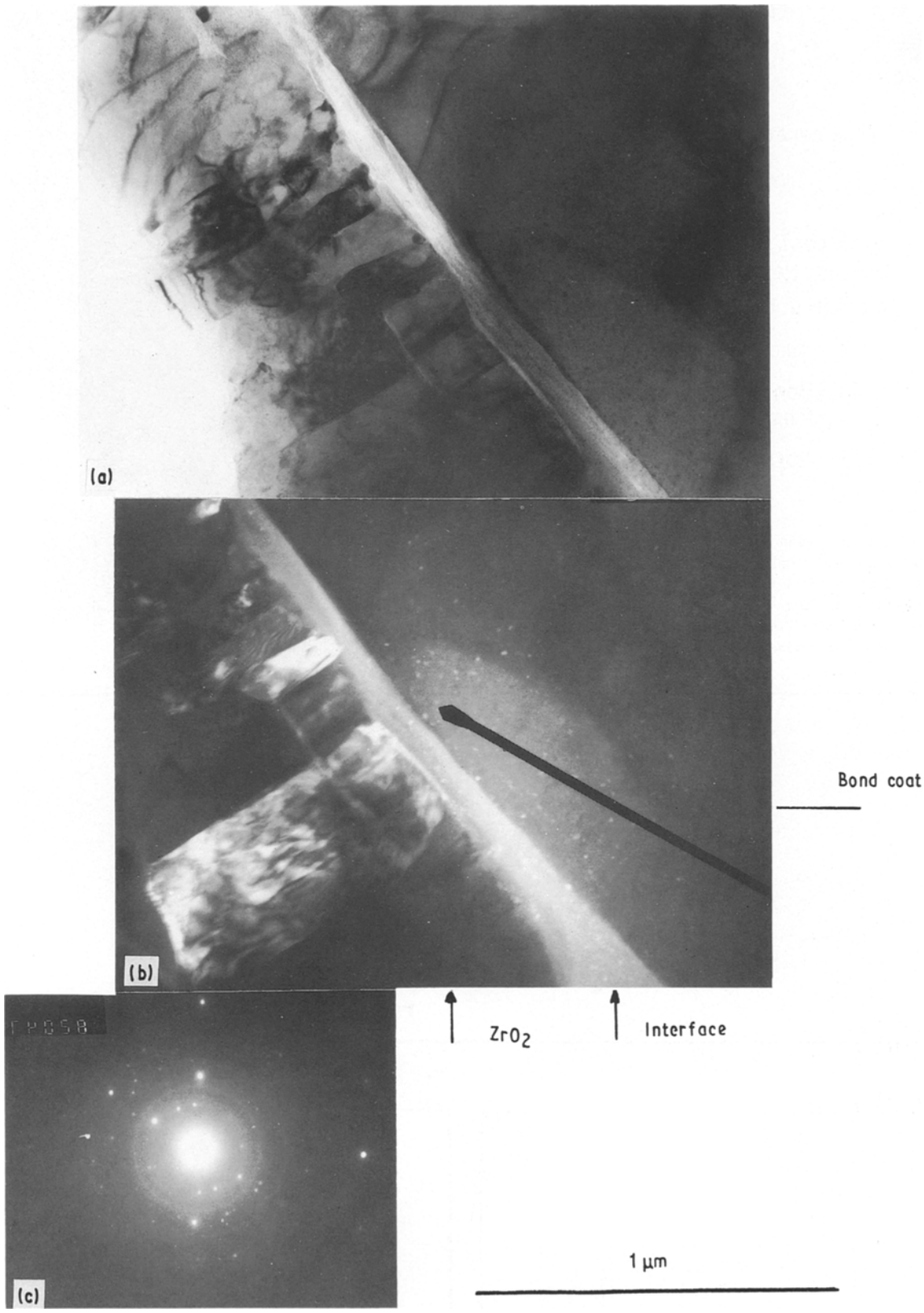

Figure 11 TEM (a) bright-field (b) dark-field images of the interfacial region between the bond coat and ceramic layer. The SAD pattern (c) gives rise to a series of faint rings, indicating the amorphous nature of the interfacial layer. Part of a ring has been imaged in the dark field (b) and shows the interface in bright contrast.

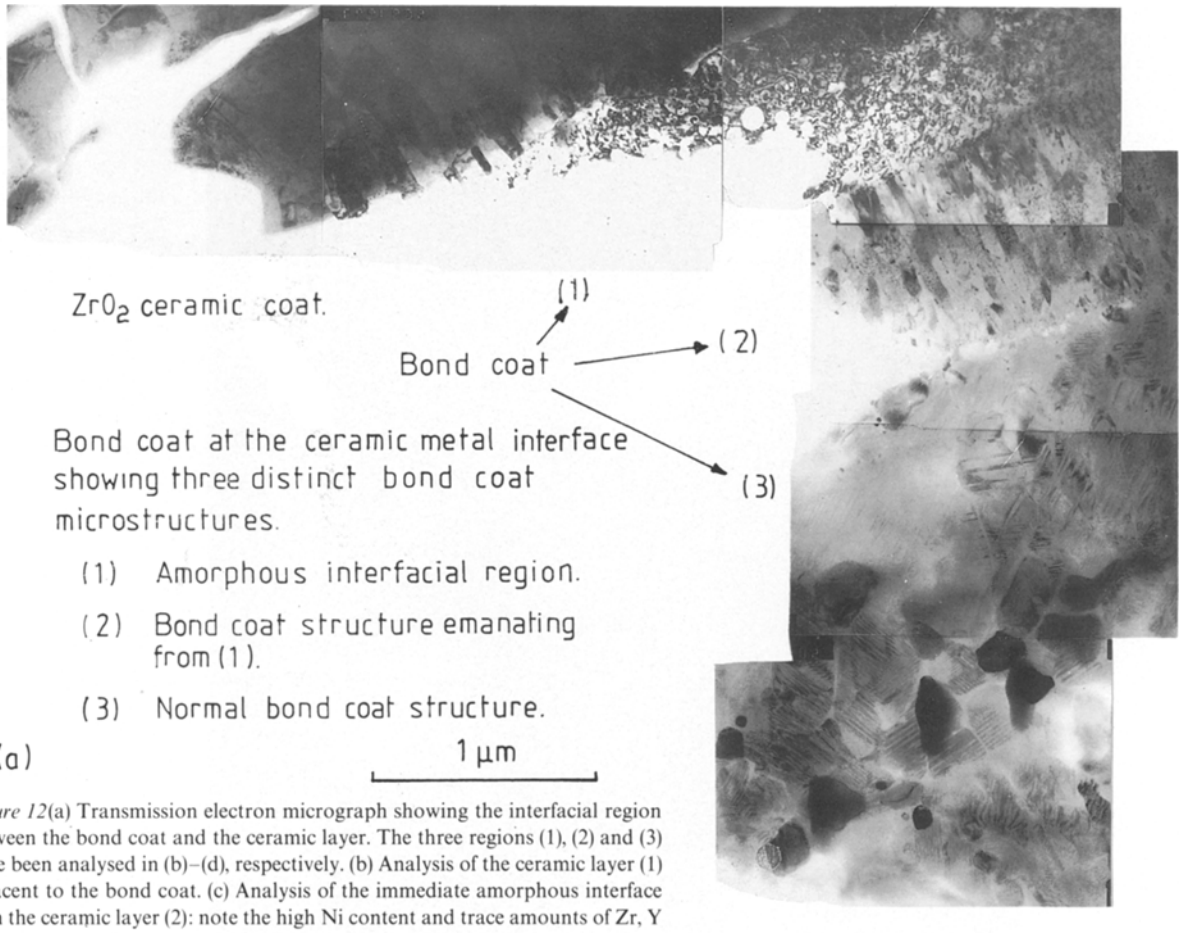

Figure 12(a) Transmission electron micrograph showing the interfacial region between the bond coat and the ceramic layer. The three regions (1), (2) and (3) have been analysed in (b)–(d), respectively. (b) Analysis of the ceramic layer (1) adjacent to the bond coat. (c) Analysis of the immediate amorphous interface with the ceramic layer (2): note the high Ni content and trace amounts of Zr, Y and Si (d) Analysis of bond coat layer (3) containing Ni, Cr and Al.

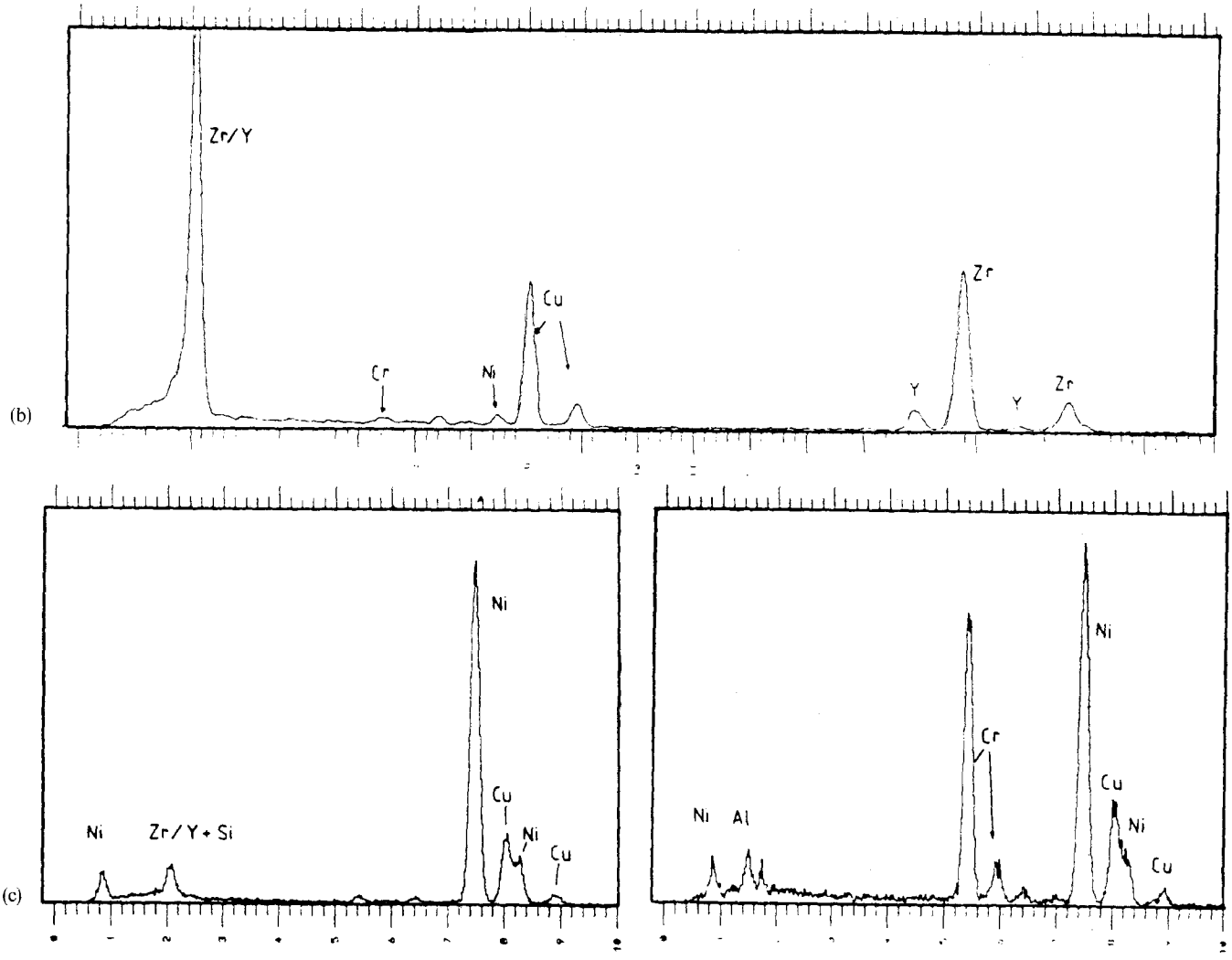

plasma gun. The slower cooling rate of this larger deposition volume of material helps to promote the formation of larger columnar and equiaxed grains. A fine columnar grain structure can still be observed in this region, but in this case it is thought to arise from rapid cooling of the thin periphery regions of a splat into the surrounding air rather than by conduction into the heat sink of the substrate. Similar large equiaxed grains have been observed by Wilms [20] in an alumina coating. These only appeared after the addition of small amounts of yttria. Their formation was therefore attributed to either grain-boundary pinning by yttria and other impurities, or alternatively to a reduction in the columnar grain growth rate, because diffusion must now take place at the growing interface.

2.7.3. Grain-boundary glassy phase

In larger grained regions, evidence for a thin continuous grain-boundary glassy phase could be found, which was observed to be concentrated at triple grain points, resulting in the rounding of the grain corners. The small quantity of this phase, coupled with its preferential etching during ion-beam thinning, has made it difficult to image the SAD pattern. For the same reasons it was not possible to identify its composition using EDX. The bright-field image in Fig. 13 does, however, show the extension of a small pocket of material from the triple point along the grain boundary.

It is suggested that this grain-boundary glassy phase is similar to that observed in fully dense PSZ and TZP ceramics sintered from powders of similar composition [23]. As analysis of the grain-boundary glassy phase in TZP material suggested that it arose from SiO_2, TiO_2 and Al_2O_3 impurities contained in the original starting powders. Such impurities were found to improve densification significantly, helping to form a liquid phase at the sintering temperature.

2.8. Effect of microstructure on properties

The amorphous interfacial layer is believed to contribute to the considerable adhesive strength of the plasma-sprayed coatings. Fracture toughness studies, using techniques such as the double cantilever beam [24, 25], have shown that when a crack is initiated at the bond coat/ceramic interface, the fracture path on delamination of the coating rarely follows the line of the interface. The fracture path tends to follow a mixed mode of bond coat and ceramic failure, the crack propagating between the lamellae of both layers [26]. These investigations suggest that the amorphous interfacial layer provides a much stronger interfacial bond than is observed between the lamellae of either the bond coat or the ceramic. When a crack is initiated along the bond coat/ceramic interface, it will tend to be deflected either into the bond coat or the ceramic, following a path of lowest interfacial strength.

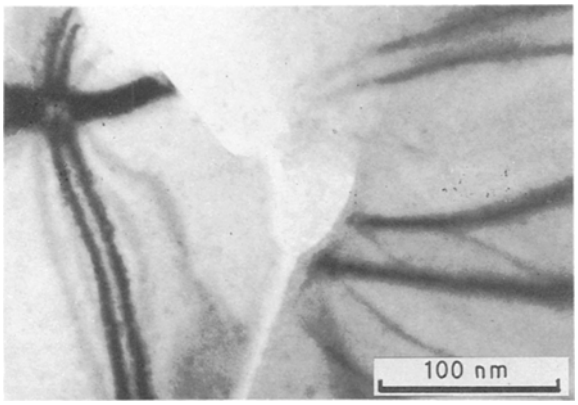

Figure 13 Transmission electron micrograph showing extension of the grain-boundary glassy phase from a tiple point along a grain boundary.

3. Conclusions

The coatings have been found to consist of a lamellar microstructure, composed of columnar and equiaxed grains. The size and shape of the grains were related to the rate of heat removal from deposited material during the coating operation, which varied through the thickness. An amorphous interfacial region between the bond coat and the ceramic has been identified; this was believed to contribute to the high adhesive strength of the ceramic layer. The compliance of the coating with the substrate is believed to result from the combination of: (1) weak bonding between the lamellae of the ceramic layer, due to the presence of interlamellar porosity, and (2) grain-boundary microcracking of the lamellae along a thin layer of intergranular glassy phase.

Acknowledgements

The authors thank SERC and Rolls Royce plc for support during this research, and Dr Paul Morrell for his help in coordinating specimen manufacture.

References

1. R. A. MILLER, S. R. LEVINE and S. STEEWA, Al AA80-0302 (1980).
2. R. A. MILLER, S. R. LEVINE and P. E. HODGE, "*Superalloys*" (American Society for Metals, 1980) p. 433.
3. P. MORRELL, PhD thesis, UMIST (1985).
4. K. MARALEEDHARAN *et al.*, *J. Amer. Ceram. Soc.* **71** (1982) C-226.
5. S. L. SHINDE and L. C. DeJONGHE, *J. Electron Micro. Tech.* **3** (1986) 361.
6. M. I. MANNING and P. C. ROWLANDS, *Brit. Corros. J.* **15** (1984) 184.
7. J. C. BRAVMAN and R. SINCLAIR, *J. Electron Micro. Tech.* **1** (1984) 53.
8. C. S. BAXTER, S. B. NEWCOMB and W. M. STUBBS, *Inst. Phys. Conf. Ser.* **68** (1984) 319.
9. B. TRUCK and B. OBERLANDER, *M.R.S. Europe* (1985) 221.
10. S. SAFAI and H. HERMAN, Conference Proceeding, Welding Institute (1978) p. 347.
11. H. MEYER, *Deut. Keram. Gesell. Ber.* **41** (1964) 112.
12. C. C. BERNDT and R. McPHERSON, *Mater. Sci. Res.* **19** (1985) 265.
13. P. BOCH *et al.*, *Adv. Ceram.* **12** (1984) 488.
14. V. H. S. WILMS, PhD thesis, University of New York, Stony Brook (1981).

15. R. McPHERSON, *J. Mater. Sci.* **15** (1980) 3141.
16. *Idem, Thin Sol. Films* **83** (1981) 297.
17. R. C. RAHL, *Mater. Sci. Engng* **1** (1966/67) 311.
18. S. SAFAI and H. HERMAN, *Thin Sol. Films* **45** (1977) 295.
19. D. TURNBULL, *J. Chem. Phys.* **18** (1950) 768.
20. V. H. S. WILMS, *Thin Sol. Films* **39** (1976) 251.
21. G. LORIMER and G. CLIFF, in "Proceedings of the 5th European Conference on Electron Microscopy" (Institute of Physics, London, 1972) p. 203.
22. A. VARDELLE, M. VARDELLE, R. McPHERSON and P. FAUCHAIS, in "9th International Thermal Spray Conference", Paper 30 (1980) p. 155.
23. M. RUHLE, N. CLAUSSEN and A. H. HEUER, *Adv. Ceram.* **12** (1984) 352.
24. C. C. BERNDT and R. McPHERSON, in "9th International Thermal Spray Conference" (1980) p. 310.
25. *Idem, Mater. Sci. Res.* **14** (1982) 619.
26. C. C. BERNDT and R. A. MILLER, *Ceram. Engng Sci. Proc.* **5** (1984) 479.

Received 27 July
and accepted 9 August 1990